Peer-reviewed version available at Appl. Sci. 2016, 6, 424; doi:10.3390/app6120424

Technical Note

Nonlinear Vibration Response of a Rectangular Tube with a Flexible End and Non-Rigid Acoustic Boundaries

Y. Y. Lee

Department of Civil and Architectural Engineering, City University of Hong Kong, Kowloon Tong, Kowloon, Hong Kong; bcraylee@cityu.edu.hk

Abstract: This paper addresses the analysis for the nonlinear vibration response of a rectangular tube with a flexible end and non-rigid acoustic boundaries. This is a further work of the linear structural acoustic problem in a well-known acoustic book. In fact, the acoustic boundaries of an enclosed space sometimes are non-rigid and the structural vibration responses are nonlinear. These two points are the focuses of this paper. The multi-level residue harmonic balance method is applied to this nonlinear structural acoustic problem. The results obtained from the multi-level residue harmonic balance method and numerical method are generally in good agreement. The effects of excitation magnitude, tube length, and phase shift parameter etc. are examined.

Keywords: nonlinear plate vibration; structural acoustics; harmonic balance method

1. Introduction

In the well-known acoustic text book [1], an investigation of resonating tube/pipe accounted for the properties of the mechanical driver, which was driven by external excitation. In the system shown in Figure 1a, there is a coupling between a linear spring-mass and an internal cavity with rigid acoustic boundaries. Similar to other structural-acoustic problems, the aforementioned problem did not consider the structural nonlinearity and non-rigid acoustic boundary. In fact, there have been many research works about linear structural-acoustics (e.g., [2-4]) and non-linear structural vibrations (e.g. [5-7]). Thus, this paper would focus on structural nonlinearity and non-rigid acoustic boundary. Besides, the multi-level residue harmonic balance method, which was developed by Leung and Guo [8] in 2011, and then modified by Hansan *et al.* [9] in 2013, is employed to solve the nonlinear differential equations, which represent the large amplitude structural vibration of a flexible panel coupled with a cavity. When compared with the classical harmonic balance method, this harmonic balance method requires less computational effort. It is because it requires to solve one nonlinear algebraic equation and one set of linear algebraic equations only for obtaining each higher level solution to any desired accuracy. Parametric studies are performed and the effects of various parameters on the nonlinear vibration responses are investigated in detail.

2. Theory

In Figure 1b, the acoustic pressure within the rectangular tube is given by the following homogeneous wave equation [1,2,10,11].

$$\nabla^2 P^h - \frac{1}{C_a^2}\frac{\partial^2 P^h}{\partial t^2} = 0 \tag{1}$$

where P^h is the h-th harmonic component of the acoustic pressure within the cavity; C_a is the speed of sound.

Preprints (www.preprints.org) | NOT PEER-REVIEWED | Posted: 18 November 2016 doi:10.20944/preprints201611.0098.v1

Peer-reviewed version available at Appl. Sci. 2016, 6, 424; doi:10.3390/app6120424

In Figure 1c, the boundary conditions of the perfectly rigid and fully open cases at $x = 0$ and a; $y = 0$ and b are given by

$$\frac{\partial P^h}{\partial x} = \frac{\partial P^h}{\partial y} = 0, \text{ for perfectly rigid} \quad (2a)$$

$$P^h = 0, \text{ for fully open} \quad (2b)$$

According to equations (2a-b) the acoustic pressure mode shapes of the perfectly rigid and fully open cases are given by

$$\varphi_{uv}(x,y) = cos\left(\frac{u\pi}{a}x\right) cos\left(\frac{v\pi}{b}y\right) \quad (3a)$$

$$\varphi_{uv}(x,y) = sin\left(\frac{(u+1)\pi}{a}x\right) sin\left(\frac{(v+1)\pi}{b}y\right) \quad (3b)$$

where $\varphi_{uv}(x,y)$ is the (u,v) acoustic mode. a and b are the cross section dimensions of the duct. u and v are the acoustic mode numbers.

Hence, the acoustic pressure mode shape of non-rigid case is defined by

$$\varphi_{uv}(x,y) = cos\left(\frac{(u+\eta)\pi}{a}x - \eta\frac{\pi}{2}\right) cos\left(\frac{(v+\eta)\pi}{b}y - \eta\frac{\pi}{2}\right) \quad (4)$$

where $\eta = \frac{\theta}{90}$; θ is the phase shift parameter. If η is set as zero in equation (4), then the acoustic mode shapes become those in the perfectly rigid case.
The boundary conditions at $z = l$ and 0 are given by

$$\frac{\partial P^h}{\partial z} = -\rho_a \frac{\partial^2 w_c^h}{\partial t^2} \text{ at } z = l \quad (5a)$$

$$P^1 = P_o \sin(\omega t) \text{ at } z = 0, \text{ for } h = 1 \quad (5b)$$

$$P^h = 0 \text{ at } z = 0, \text{ for } h \neq 1 \quad (5c)$$

where l is the duct length; ρ_a = air density; ω is the excitation frequency As that the external sound pressure at $z = 0$ is a simple harmonic excitation (i.e. no higher harmonic components). P_o is the sound excitation magnitude, $\gamma \times P_{ref}$; γ is the dimensionless parameter; P_{ref} is the reference pressure level, 2×10^{-5} N/m^2. $w_l^h(x,y,t)$= the h^{th} harmonic component of the nonlinear panel displacement at $z = l$.

$$w_l^h(x,y,t) = A_{h,sin}(t)\phi_{mn}(x,y) \quad (6)$$

where $\phi_{mn}(x,y) = \sin\left(\frac{m\pi x}{a}\right)\sin\left(\frac{n\pi y}{b}\right)$= the (m,n) panel mode (it is simply supported). $A_{h,sin}(t) = A_h \sin(h\omega t)$; A_h is the panel vibration amplitude. The total response of the panel is equal to the summation of all harmonic components and given by

$$w_l(x,y,t) = \sum_{h=1,3,5\ldots}^{H} w_l^h(x,y,t) = \sum_{h=1,3,5\ldots}^{H} A_{h,sin}(t)\phi_{mn}(x,y) \quad (7)$$

where $w_c(x,y,t)$ is the total response of the panel at $z = l$. H = the number of harmonic terms. Then, the multi-level residue harmonic balance method is adopted for solving the differential equations and obtaining the unknown panel displacement responses. For simplicity, only the zero, 1st and 2nd level solution procedures (or three harmonic components are considered) are showed here. According to the multi-level residue harmonic balance solution form proposed in [9,12],

$$A(t) = \varepsilon^0 A0(t) + \varepsilon A1(t) + \varepsilon^2 A2(t) \quad (8)$$

Preprints (www.preprints.org) | NOT PEER-REVIEWED | Posted: 18 November 2016 doi:10.20944/preprints201611.0098.v1

Peer-reviewed version available at Appl. Sci. 2016, 6, 424; doi:10.3390/app6120424

where ε is an embedding parameter. Any terms associated with ε^0, ε^1, ε^2 represent those terms considered in the zero, 1st, and 2nd level solution procedures respectively. Then, the zero, 1st and 2nd level solutions, $A0(t)$, $A1(t)$, and $A2(t)$ are given by

$$A0(t) = A0_1 \sin(\omega t)$$

$$A1(t) = A1_1 \sin(\omega t) + A1_3 \sin(3\omega t)$$

$$A2(t) = A2_1 \sin(\omega t) + A2_3 \sin(3\omega t) + A2_5 \sin(5\omega t) \quad \text{(9a-c)}$$

The 1st, 2nd, and 3rd harmonic components of the total displacement amplitude, A_1, A_2, and A_3 are given by

$$A_1 = A0_1 + A1_1 + A2_1; \quad A_3 = A1_3 + A2_3 \; ; \quad A_5 = A2_5 \quad \text{(10a-c)}$$

Then, the solution form of the acoustic pressure in equation (1) is given by [1,2,10-12]

$$P^h(x,y,z,t) = \sum_u^U \sum_v^V [L_{uv}^h \sinh(\mu_{uv}^h z) + N_{uv}^h \cosh(\mu_{uv}^h z)] \, \varphi_{uv}(x,y) sin(h\omega t) \quad (11)$$

where $\mu_{uv}^h = \sqrt{\left(\frac{(u+\eta)\pi}{a}\right)^2 + \left(\frac{(v+\eta)\pi}{b}\right)^2 - \left(\frac{h\omega}{c_a}\right)^2}$; L_{uv}^h and N_{uv}^h are coefficients that depend on the boundary conditions at $z = 0$ and $z = l$; U and V are the numbers of acoustic mode numbers used.

The unknown coefficients L_{uv}^h and N_{uv}^h can be obtained by applying the boundary condition at $z = 0$ and $z = l$ in equations (5a-c) to equation (11). They are given by for $h = 1$, $N_{uv}^1 = P_o \frac{\alpha_{uv}^0}{\alpha_{uv}^{uv}}$ and $L_{uv}^1 = \rho_a \frac{\omega^2 A_1}{\mu_{uv}^1 \cosh(\mu_{uv}^1 l)} \frac{\alpha_{uv}^{mn}}{\alpha_{uv}^{uv}} - P_o \frac{\alpha_{uv}^0}{\alpha_{uv}^{uv}} \tanh(\mu_{uv}^1 l)$; for $h \neq 1$, $N_{uv}^h = 0$ and $L_{uv}^h = \frac{\rho_a (h\omega)^2}{\mu_{uv}^h} \frac{1}{\alpha_{uv}^{uv}} \left(\frac{\alpha_{uv}^{mn} A_h}{\cosh(\mu_{uv}^h l)}\right)$; $\alpha_{uv}^o = \int_0^b \int_0^a \varphi_{uv} dxdy$; $\alpha_{uv}^{uv} = \int_0^b \int_0^a \varphi_{uv} \varphi_{uv} dxdy$; $\alpha_{uv}^{mn} = \int_0^b \int_0^a \varphi_{uv} \phi_{mn} dxdy$; $\alpha_{mn}^{mn} = \int_0^b \int_0^a \phi_{mn} \phi_{mn} dxdy$.

Once L_{uv}^h and N_{uv}^h are obtained, the modal pressure force magnitude at $z = l$ can be found using equation (11)

$$\overline{P}_l^1 = K_A^1 A_1 + K_o^1 P_o \; , \text{for } h = 1 \quad \text{(12a)}$$

$$\overline{P}_l^h = K_A^h A_h \, , \text{for } h \neq 1 \quad \text{(12b)}$$

where $K_A^1 = \sum_u^U \sum_v^V \frac{\rho_a \omega^2}{\mu_{uv}^1} \frac{(\alpha_{uv}^{mn})^2}{\alpha_{uv}^{uv} \alpha_{mn}^{mn}} \tanh(\mu_{uv}^1 l)$; $K_o^1 = \sum_u^U \sum_v^V \frac{\alpha_{uv}^{mn} \alpha_{uv}^o}{\alpha_{mn}^{mn} \alpha_{uv}^{uv}} \frac{1}{\cosh(\mu_{uv}^1 l)}$;

In this study, the nonlinear free vibration formulation of panel adopted in [38] is employed.

$$\rho_l \frac{d^2 A}{dt^2} + \rho_l \omega_l^2 A + \beta_l A^3 = 0 \quad (13)$$

where ρ_l and ω_l are the surface density and linear resonant frequency of the panel; β_l represents the nonlinear stiffness coefficient due to the large amplitude vibration.

$$\beta_l = \frac{E\tau}{4(1-\nu^2)} \left(\frac{m\pi}{a}\right)^4 \left[\left(1 + \left(\frac{n}{m} r\right)^4\right)\left(\frac{3}{4} - \frac{\nu^2}{4}\right) + \nu \left(\frac{n}{m} r\right)^2\right] \quad (14)$$

where $r = a/b$ is the aspect ratio; ν is the Poisson's ratio. E is the Young's modulus. is the panel thickness.

By putting the acoustic force terms developed from equations (12a-b) into (13), the governing equation for the nonlinear forced vibrations is given by

Preprints (www.preprints.org) | NOT PEER-REVIEWED | Posted: 18 November 2016 doi:10.20944/preprints201611.0098.v1

Peer-reviewed version available at Appl. Sci. 2016, 6, 424; doi:10.3390/app6120424

$$\rho_l \frac{d^2A}{dt^2} + \rho_l \omega_l^2 A + \beta_l A^3 + \sum_{h=1,3,5\ldots}^{H} K_A^h A_h \sin(h\omega t) = K_o^1 P_o \quad \sin(\omega t) \tag{15}$$

Substitute equation (9) into (15) and consider those terms associated with ε^0. Then consider the harmonic balance of $\sin(\omega t)$. The zero level equation without the damping term is given by

$$(K_A^1 + \Pi(\omega))A0_1 \; + \frac{3}{4}\beta_l A0_1^3 = K_o^1 P_o \tag{16}$$

where $\Pi(\omega) = \rho_l\left(-\omega^2 \; + \omega_l^2\right)$; The unbalanced residual in the zero level procedure is $\Delta_{A0} = -\frac{1}{4}\beta_l A0_1^3 \sin(3\omega t)$

According to equation (16), the damped vibration amplitude is given in the following form

$$A0_1 = \frac{K_o^1 P_o}{(K_A^1 + \pi(\omega)) + \frac{3}{4}\beta_l |A0_1|^2} \tag{17}$$

where $\Pi(\omega) = \rho_l\left(-\omega^2 \; + \omega_l^2\right) + j(C_a \rho_a \omega + \xi \omega \omega_p)$; $j = \sqrt{-1}$; ξ is the internal material damping coefficient; ω_p is the nonlinear resonant peak frequency; "$C_a \rho_a \omega$" represents the radiation damping term [1,13].

Again, substitute equation (9) into (15) and consider those terms associated with ε^1 to obtain the following 1st level equation

$$(K_A^1 + \pi(\omega))A1_1 \sin(\omega t) + (K_A^3 + \pi(3\omega))A1_3 \sin(3\omega t) + 3\beta_l (A0)^2 A1 + \Delta_{A0} = L_1 \tag{18}$$

where L_1 represents the summation of the 1st level terms and the unbalanced residual in the zero level. Δ_{A0} is the residual in the zero level.

Then, consider the harmonic balances of $\sin(\omega t)$ and $\sin(3\omega t)$ for equation (18)

$$\int_0^{2\pi} L_1 \sin(\omega t) dt = 0; \; \int_0^{2\pi} L_1 \sin(3\omega t) dt = 0 \tag{19a-b}$$

Hence, $A1_1$ and $A1_3$ can be found by solving equation (19a-b).

Similarly, substitute equation (9) into (15) and consider those terms associated with ε^2 to obtain the following 2nd level equation

$$(K_A^1 + \pi(\omega))A2_1 \sin(\omega t) + (K_A^3 + \pi(3\omega))A2_3 \sin(3\omega t) + (K_A^5 + \pi(5\omega))A2_5 \sin(5\omega t) + 3\beta_c A0(A1)^2 + 3\beta_l A2(A0)^2 + \Delta_{A1} = L_2 \tag{20}$$

where L_2 represents the summation of the 2nd level terms and the unbalanced residual in the 1st level. Δ_{A1} is the residual in the zero level.

Then, consider the harmonic balances of $\sin(\omega t)$, $\sin(3\omega t)$, and $\sin(5\omega t)$ for equation (20)

$$\int_0^{2\pi} L_2 \sin(\omega t) dt = 0 \int_0^{2\pi} L_2 \sin(3\omega t) dt = 0; \int_0^{2\pi} L_2 \sin(5\omega t) dt = 0 \tag{21a-c}$$

Hence, $A2_1$, $A2_3$, and $A2_5$ can be found by solving equations (21a-c).

3. Results and Discussion

In this section, the material properties in the numerical cases are as follows: Young's modulus = 7.1×10^{10} N/m^2, Poisson's ratio = 0.3, and mass density = 2700 kg/m^3 ; panel dimensions = 0.4m × 0.4m × 2m; damping ratio ξ = 0.02. Tables 1a-c show the convergence studies of normalized panel vibration amplitude for various excitation magnitudes and frequencies. The 9 acoustic mode solutions, 3 structural mode solutions, and 2nd level solutions are normalized as one hundred. The acoustic boundaries are rigid (i.e. =0). In Tables 1a-c, the first 9 symmetrical acoustic modes, the first 3 structural modes are used for checking. The zero, 1st and 2nd level solutions contain 1, 2, and 3 harmonic components, respectively (i.e $\sin(\omega t)$, $\sin(3\omega t)$, and $\sin(5\omega t)$). It is shown that the 1st level 4 acoustic mode and two structural mode approach is good enough for convergent and accurate vibration amplitude solution.

Figures 2a-c present the comparisons between the vibration amplitudes obtained from the present harmonic balance method and numerical method used in [6]. The results obtained from the two methods are generally in good agreement. Relatively, the agreement in Figure 2a is the best because of smaller nonlinearity. In Figures 2b-c, there are somewhat deviations observed around the major peak values. Note that there are some minor peaks around ω/ω_l = 2.3 and 3.4 in Figure 2c. In these three cases, the first acoustic resonances occur around ω/ω_l = 1.4. In the case of , the well-known jump phenomena, which are due to the first structural resonance and higher acoustic resonances, occurs around ω/ω_l = 2.3, 3.9 and 4.5 (see Points A, B and C). The solution line discontinues there. There is a trough on the solution line around ω/ω_l = 4.2. In the cases of and 8, the jump phenomena due to the first structural resonance and higher acoustic resonances occur at the higher frequencies. Unlike the trough on the solution line in the case of a small peak and a large peak occur on the solution lines of and 8 around ω/ω_l = 4.2, respectively. Besides, Points A and B in the case of are very close. There is no Points A and B in the case of it is because of no discontinuous portion on the solution line there).

Figure 3 shows the vibration amplitude plotted against the excitation frequency for various tube lengths. The first peak value due to the acoustic resonance and first jump down frequency increase with the tube length, while the first peak frequency and the first trough frequency decrease with the tube length. In the case of l=10a, the tube length is the longest among the three cases. Thus, the second peak occurs around ω/ω_l = 2.1, which is lower than the first jump down frequency; and there are more acoustic resonant peaks on the solution line. In the case of l=3a, the tube length is the shortest among the three cases. The trough occurs out of the frequency range (i.e. ω/ω_l > 6).
Figure 4 shows the vibration amplitude plotted against the excitation frequency for various phase shift parameters. The first peak frequency due to the acoustic resonance, the first jump down frequency and the trough frequency increase with the phase shift parameter, while the first peak value decreases with the tube length. In the cases of = 5 and 10, it is implied that the tube boundaries are not perfectly rigid and the corresponding air particle velocities are non-zero. It is noted that the first peak is quite small, marginally detectable when the phase shift is only 8 degree.
Besides, the phase shift does not significantly the higher acoustic resonances. Figure 5 show the vibration amplitude plotted against the excitation frequency for the tubes filled with air and CO_2. The density of CO_2 and the corresponding sound speed are about 50% higher than those in the case of air. There are big difference between the two cases. In case of CO_2, the first peak is much smaller and the jump phenomenon disappears. The peaks due to higher acoustic resonances are out of the frequency range.

4. Conclusions

This paper has presented the analysis for the nonlinear vibration response of a rectangular tube with a flexible end and non-rigid acoustic boundaries. The structural/acoustic modal formulation has been developed from the partial differential equations which represent the large amplitude structural

vibration of a flexible panel coupled with a cavity. The results obtained from the multi-level residue harmonic balance method and numerical method are generally in good agreement. The effects of excitation magnitude, tube length, and phase shift parameter etc. are investigated. It can be concluded from the results that 1) if the tube length is longer, more vibration peaks due to the acoustic resonances appear within the particular frequency range; 2) these peak values are also very sensitive to the phase shift parameter. For an example, the first peak is marginally detectable when the phase shift is only 8 degree; 3) if the tube is filled with CO_2, which density and corresponding sound speed about 50% higher than those of air, the vibration peaks become very small or disappear within the particular frequency range.

Acknowledgments
The work described in this paper was fully supported by the CityU SRG [project no. 7004701]

References

1. Kinsler, L.E.; Frey, A.R.; Coppens, A.B.; Sanders, J.V. *Fundamentals of Acoustics*, Fourth Editions; John Wiley & Sons. Inc. 2000.
2. Pretlove, A.J. Free vibrations of a rectangular panel backed by a closed rectangular cavity. *Journal of Sound and Vibration* **1965**, 2(3), 197-209.
3. Oldham, D.J.; Hillarby, S.N. The acoustical performance of small close fitting enclosures Part I Theoretical Models. *Journal of Sound and Vibration* **1991**, 150(2), 261-281.
4. Lee, Y.Y.; Lee, E.W.M. Widening the sound absorption bandwidths of flexible micro-perforated curved absorbers using structural and acoustic resonances. *International Journal of Mechanical Sciences* **2007**, 49(8), 925-934.
5. Younesian, D.; Sadri, M.; Esmailzadeh, E.: Primary and secondary resonance analyses of clamped-clamped micro-beams. *Nonlinear Dynamics*. **2014**, 76(4), 1867-1884.
6. Lee, Y.Y.; Su, R.K.L.; Ng, C.F.; Hui, C.K. The effect of the modal energy transfer on the sound radiation and vibration of a curved panel: Theory and Experiment. *Journal of Sound and Vibration* **2009**, 324, 1003–1015.
7. Lee, Y.Y.; Poon, W.Y.; Ng, C.F. Anti-symmetric mode vibration of a curved beam subject to autoparametric excitation. *Journal of Sound and Vibration* **2006**, 290(1-2), 48-64.
8. Leung, A.Y.T.; Guo, Z. Feed forward residue harmonic balance method for a quadratic nonlinear oscillator. *International Journal of Bifurcation and Chaos* **2011**, 21(6), 1783-1794.
9. Hasan, A.S.M.Z; Lee, Y.Y.; Leung, A.Y.T. The multi-level residue harmonic balance solutions of multi-mode nonlinearly vibrating beams on an elastic foundation. *Journal of Vibration and Control* **2016**, 22(14), 3218–3235 DOI: 10.1177/1077546314562225.
10. Lee, Y.Y,; Ng, C.F. Sound insertion loss of stiffened enclosure plates using the finite element method and the classical approach, *Journal of Sound and Vibration* **1998**, 217(2), 239-260.
11. Hui, C.K.; Lee, Y.Y.; Reddy, J.N. Approximate elliptical integral solution for the large amplitude free vibration of a rectangular single mode plate backed by a multi-acoustic mode cavity. *Thin-Walled Structures*, **2011**, 49(9), 1191-1194.
12. Lee, Y.Y. The effect of leakage on the sound absorption of a nonlinear perforated panel backed by a cavity. *International Journal of Mechanical Sciences* **2016**, 107, 242-252.
13. Lee, Y.Y. Multi-Level Residue Harmonic Balance Method for the Transmission Loss of a Nonlinearly Vibrating Perforated Panel. *International Journal of Structural Stability and Dynamics* **2016**, 16, Article number 1450100.

Preprints (www.preprints.org) | NOT PEER-REVIEWED | Posted: 18 November 2016 doi:10.20944/preprints201611.0098.v1

Peer-reviewed version available at Appl. Sci. 2016, 6, 424; doi:10.3390/app6120424

Table 1a Acoustic mode convergence study (1st level solution, number of structural modes =2, l= 5a, =4)

	No. of acoustic modes =		
	1	4	9
ω/ω_c=1.8	99.83	100.00	100*
2.8	99.09	99.97	100*
4.8	99.97	100.24	100*

**the amplitudes are normalized as 100*

Table 1b Structural mode convergence study (1st level solution, number of acoustic modes =4, l= 5a, =4)

	No. of structural modes =		
	1	2	3
ω/ω_c=1.8	99.20	100.00	100*
2.8	98.77	100.00	100*
4.8	70.28	99.97	100*

**the amplitudes are normalized as 100*

Table 1c Harmonic term convergence study (number of structural modes =2, number of acoustic modes =4, l= 5a, =4)

	No. of harmonic terms =		
	1 (zero level)	2 (1st level)	3 (2nd level)
ω/ω_c=1.8	103.60	100.66	100*
2.8	100.17	100.00	100*
4.8	99.83	100.00	100*

**the amplitudes are normalized as 100*

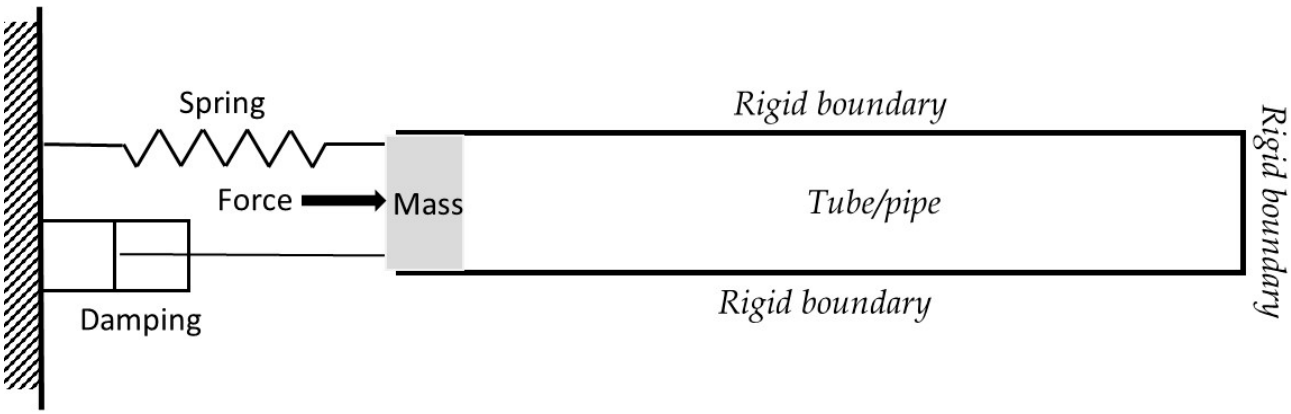

Figure 1a The linear structural-acoustic model in [1]

Preprints (www.preprints.org) | NOT PEER-REVIEWED | Posted: 18 November 2016 doi:10.20944/preprints201611.0098.v1

Peer-reviewed version available at Appl. Sci. 2016, 6, 424; doi:10.3390/app6120424

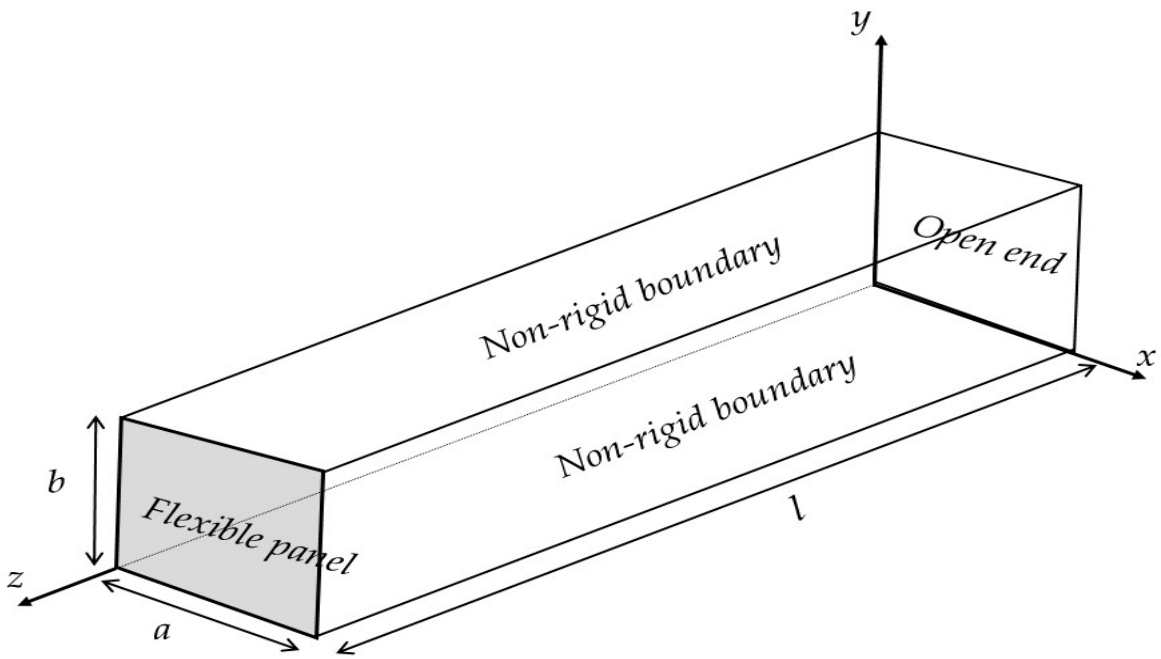

Figure 1b Schematic diagram of a rectangular tube with a flexible end and non-rigid acoustic boundaries

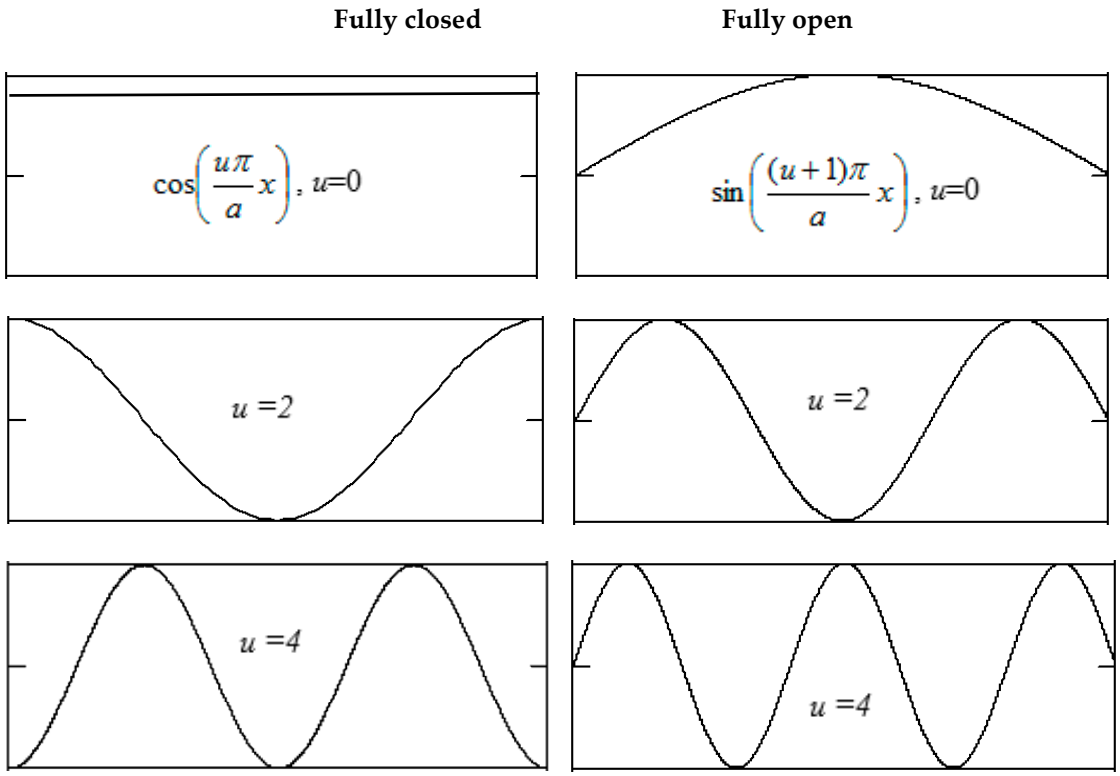

Figure 1c Acoustic mode shapes of the fully open and fully closed cavity boundaries

Preprints (www.preprints.org) | NOT PEER-REVIEWED | Posted: 18 November 2016 doi:10.20944/preprints201611.0098.v1

Peer-reviewed version available at Appl. Sci. 2016, 6, 424; doi:10.3390/app6120424

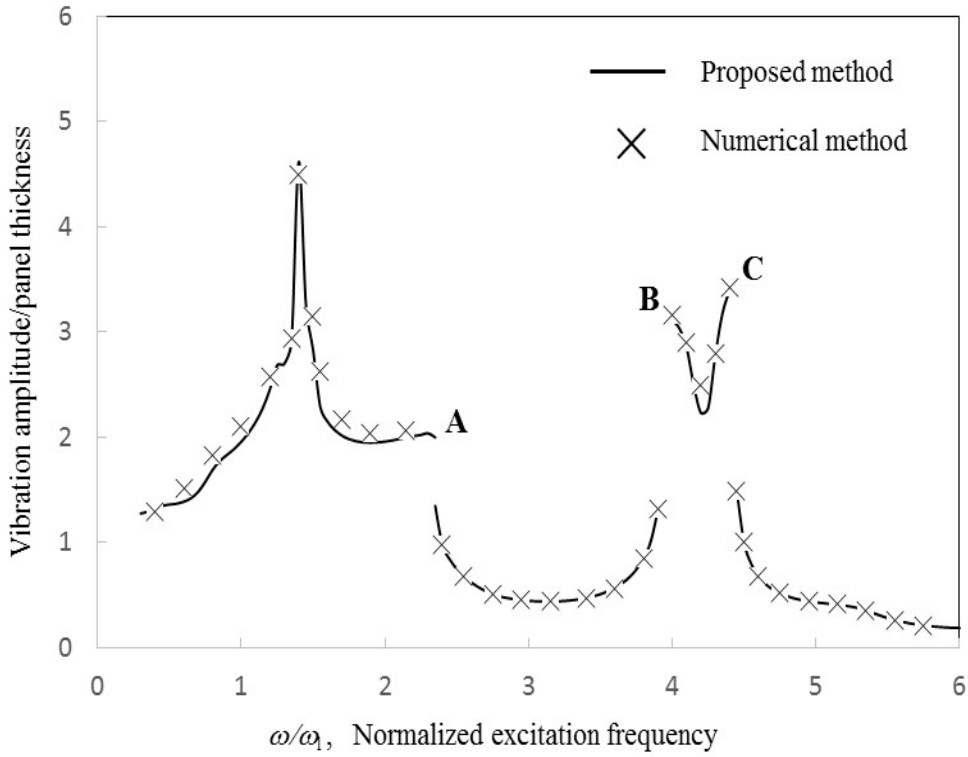

Figure 2a
Comparison between the solutions obtained from the proposed method and numerical integration method [6] (number of structural modes =2, number of acoustic modes =4, $l = 5a$, = 2, =0)

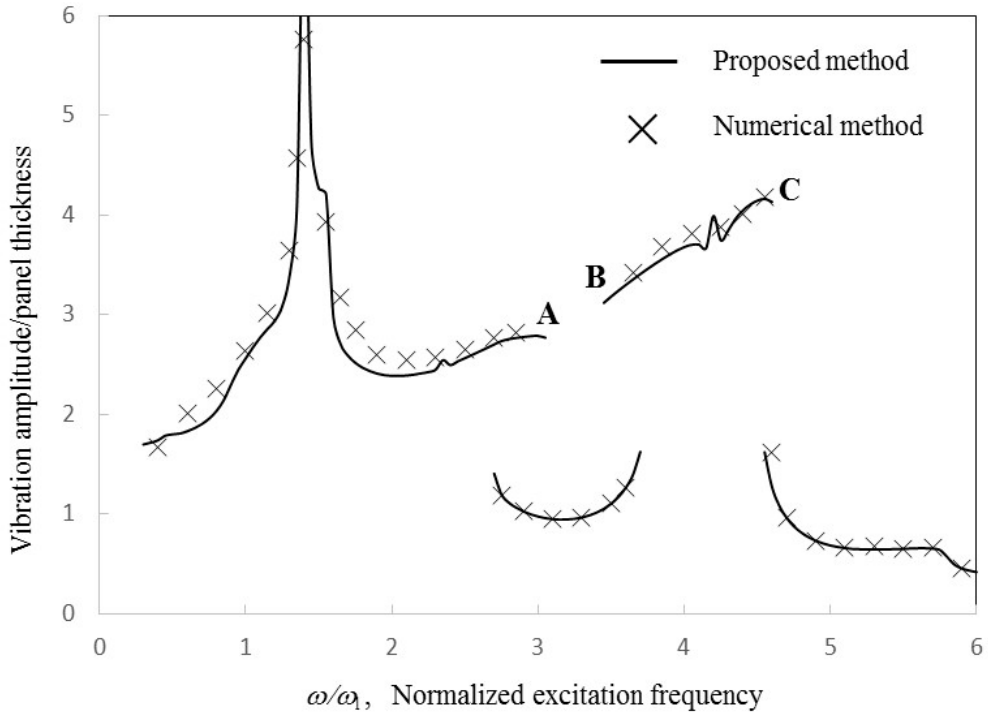

Figure 2b
Comparison between the solutions obtained from the proposed method and numerical integration method [6] (number of structural modes =2, number of acoustic modes =4, $l = 5a$, = 4, =0)

Preprints (www.preprints.org) | NOT PEER-REVIEWED | Posted: 18 November 2016 doi:10.20944/preprints201611.0098.v1

Peer-reviewed version available at Appl. Sci. 2016, 6, 424; doi:10.3390/app6120424

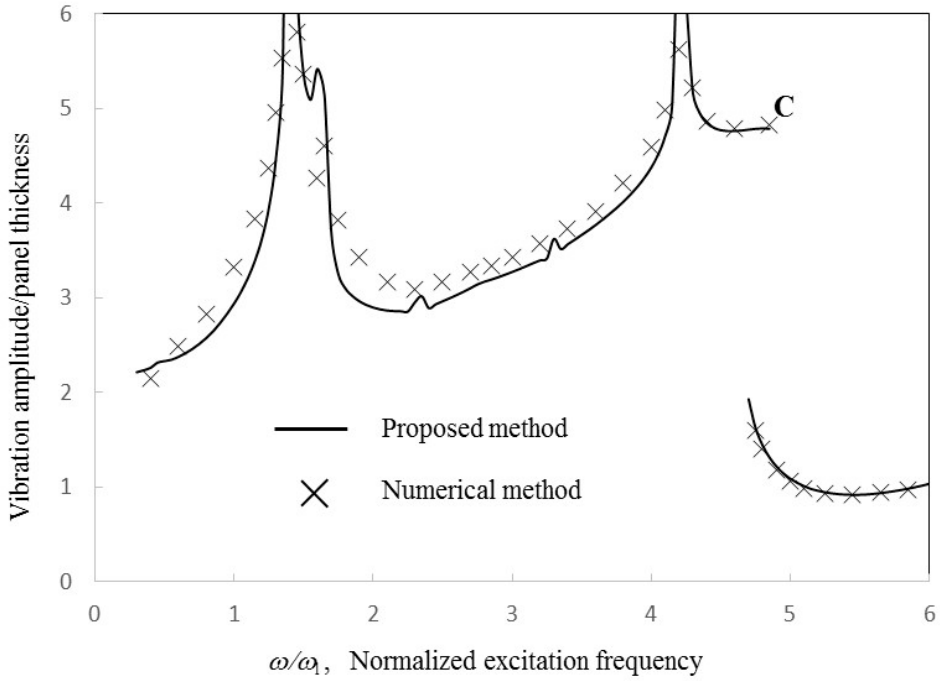

Figure 2c
Comparison between the solutions obtained from the proposed method and numerical integration method [6] (number of structural modes =2, number of acoustic modes =4, $l = 5a$, = 8, =0)

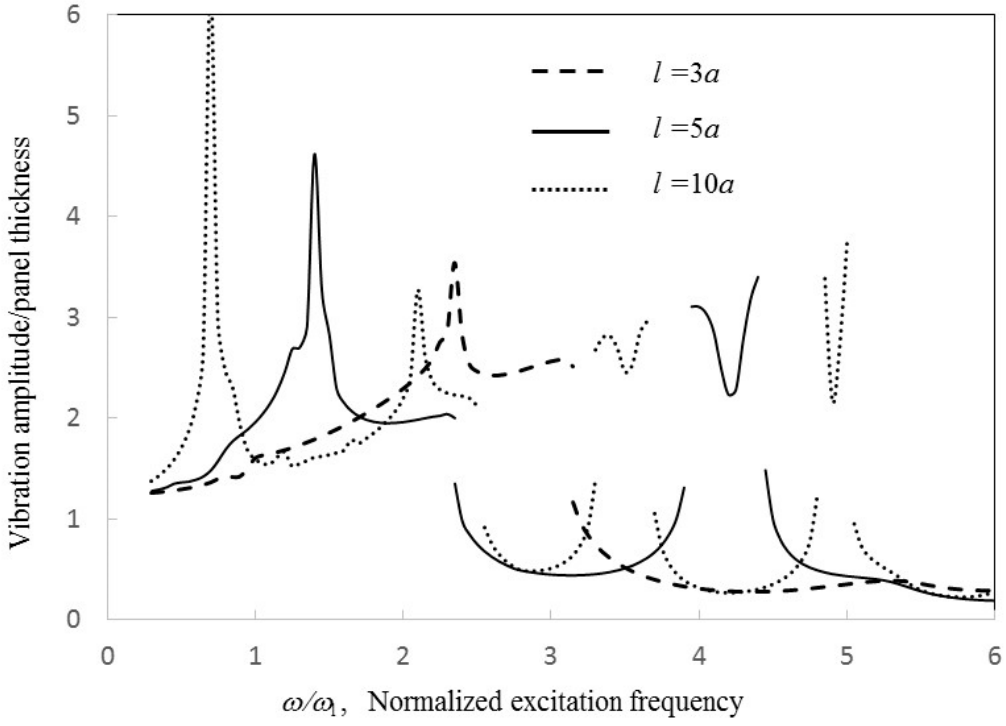

Figure 3
Vibration amplitude ratio versus normalized excitation frequency for various duct lengths (number of structural modes =2, number of acoustic modes =4, = 2, =0)

Preprints (www.preprints.org) | NOT PEER-REVIEWED | Posted: 18 November 2016 doi:10.20944/preprints201611.0098.v1

Peer-reviewed version available at Appl. Sci. 2016, 6, 424; doi:10.3390/app6120424

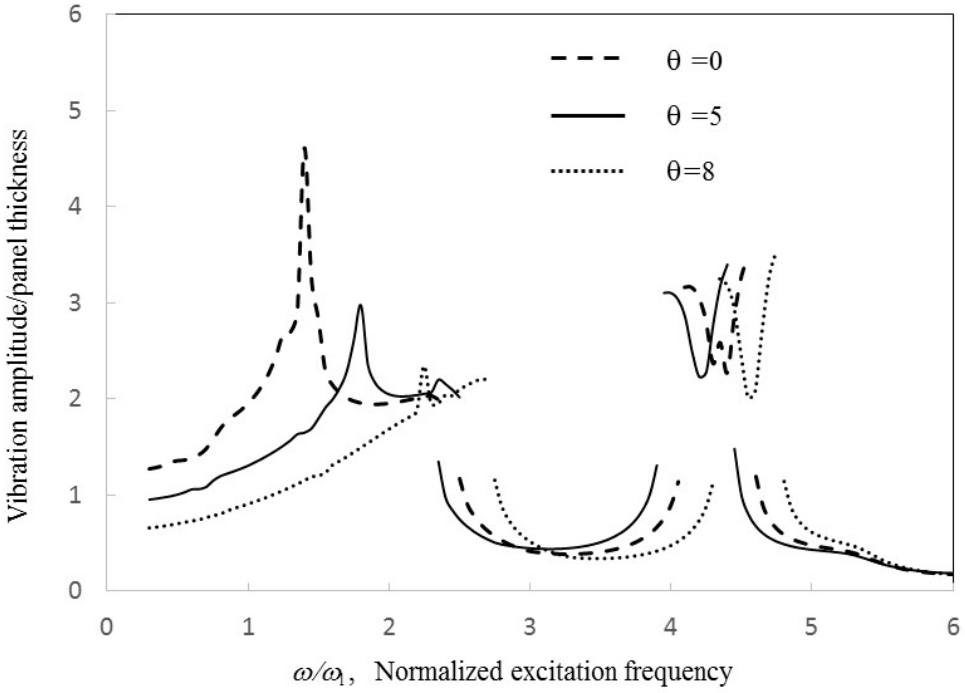

Figure 4
Vibration amplitude ratio versus normalized excitation frequency for various acoustic boundary conditions (number of structural modes =2, number of acoustic modes =4, $l = 5a$, = 2)

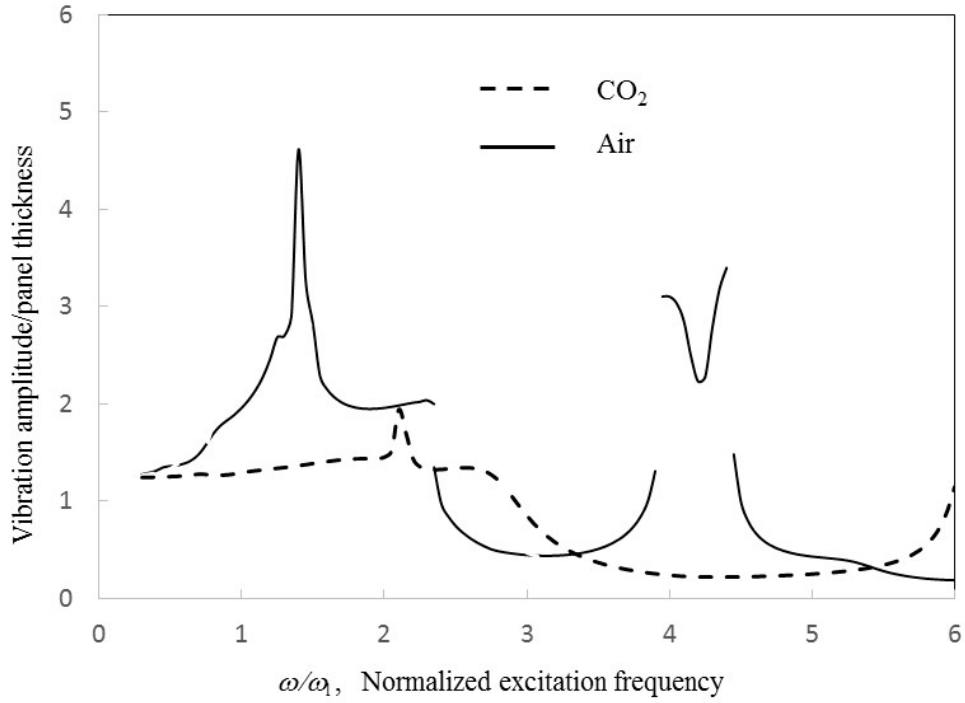

Figure 5
Vibration amplitude ratio versus normalized excitation frequency for the cases of air and CO_2 (number of structural modes =2, number of acoustic modes =4, $l = 5a$, = 2, =0)